

Spectroscopic factors of resonance states with the Gamow shell model

M. R. Xie,^{1,2} J. G. Li,^{1,2,*} N. Michel,^{1,2} H. H. Li,^{1,2} and W. Zuo^{1,2}

¹*Institute of Modern Physics, Chinese Academy of Sciences, Lanzhou 730000, China*

²*School of Nuclear Science and Technology, University of Chinese Academy of Sciences, Beijing 100049, China*

(Dated: May 18, 2023)

We provide an investigation of the spectroscopic factors of resonance states in $A = 5 - 8$ nuclei using two distinct nuclear models, the Gamow shell model (GSM) and the no-core shell model (NCSM). Configuration mixing is treated exactly in both GSM and NCSM. GSM employs the complex-energy Berggren ensemble, which treats bound, unbound resonance, and non-resonant continuum single-particle states on an equal footing. As a result, continuum coupling is taken into account in GSM, whereas it is absent in NCSM, where the harmonic oscillator basis is used. We first calculate low-lying states of helium isotopes and isotones. The results indicate that GSM can more accurately reproduce the low-lying resonance states than NCSM. The spectroscopic factors of the resonance states are also computed. Results from the GSM and NCSM are compared and show that continuum coupling plays an important role in the calculations of spectroscopic factors of resonance states. Overlap functions related to the resonance states are also systematically calculated by the GSM and NCSM. It is then demonstrated that wave function asymptotes can only be reproduced in GSM, where continuum coupling is taken into account.

I. INTRODUCTION.

Large scientific facilities have been upgraded or are being constructed, such as the facility for rare isotope beams (FRIB), RI Beam Factory (RIBF), the Heavy Ion Research Facility in Lanzhou (HIRFL), and High Intensity Heavy-ion Accelerator Facility (HIAF), which have advanced the study of exotic nuclei away from the valley of stability and propelled it to the forefront of nuclear physics research. The peculiar phenomena that distinguish unstable nuclei from those close to the valley of stability include shell evolution [1, 2], halo and skin nuclei [3, 4], exotic decay such as two-proton or two-neutron radioactivity [5–8], etc. Such phenomena occur as a consequence of valence nucleons primarily occupying shells near particle-emission threshold. The study of the structure of exotic nuclei has generated great interest both theoretically and experimentally. Many works have already been done on these subjects, particularly about halo nuclei [9–12]. However, some questions remain unanswered regarding the coupling of resonance and scattering states above particle-emission threshold [13], while relevant experimental data are lacking or even unavailable. Resonance nuclei located far from the valley of stability and close to, or beyond drip-line, form a basic laboratory to study the coupling of discrete states with scattering continuum states [14]. Traditional shell models have difficulties in describing the properties of these resonance nuclei. It necessitates the introduction of new and powerful models that account for the complicated interplay among the different degrees of freedom in those weakly-bound and resonance states [15, 16].

A typically feature of many-body resonance states is the strong coupling to the continuum. The coupling between the resonance states and the continuum poses the

greatest challenges in the theoretical description of unbound nuclei. Various studies have demonstrated that continuum coupling has a significant impact on the properties of the nucleus in the drip-line regions, such as energy spectra [17, 18], asymptotic normalization coefficients (ANC) [19], spectroscopic factors (SF) [20–22], etc.

In nuclear structure studies, the shell model embedded in the continuum (SMEC) [16, 23], which treats the bound states and the scattering states on an equal footing, has been developed these recent years. However, SMEC typically only allows one particle to be present in the continuum. While it is in principle possible to include two particles in the continuum in SMEC, as in the context of two-proton radioactivity [24, 25], it can only be performed with approximations, such as cluster and sequential emissions. In contrast, the Gamow shell model (GSM) used in the present work effectively avoids this defect and allows multiple particles to be present in the non-resonant continuum. GSM allows to perform many-body computations using the Gamow-Berggren basis in rigged Hilbert spaces [26–29]. The Berggren basis extends the Schrödinger equation to the complex momentum space, whereby the scattering contours associated to resonance states are discretized with the Gauss-Legendre rule. Physical quantities are complex, so that the width of resonance states is obtained from the imaginary part of energy. A variety of phenomena induced by the proximity of the nucleon-emission threshold shows that the asymptotic part of many-body wave functions must be precisely reproduced, which is the case in GSM. GSM has thus been used to investigate unbound states in drip-line nuclei, such as the conditions of the existence of a $4n$ resonance system [30], the prediction of the ground-state energy of ^{28}O [31], and the calculations of energies and widths associated to the one-proton and two-proton decays of ^{18}Mg [18, 32] and to the possibility of a narrow resonance ground state in ^7H [33].

* jianguo.li@impcas.ac.cn

SF and its associated overlap function are useful tools for the study of the structure of many-body wave functions of unbound nuclei. SF represents the amount of occupancy of a specific single-particle (s.p.) orbit and associated shell model configuration in the many-body nuclear wave function. It is also a physical quantity that connects the nuclear structure to the nuclear reaction [34–36]. However, at present, theoretical SFs differ significantly from experimental data [36–39]. Studies have also demonstrated that continuum coupling provide large contributions to SFs in resonance and weakly-bound nuclei [22, 39]. As both continuum effects and inter-nucleon correlations are taken into account simultaneously in the GSM [40], the asymptotes of many-body systems are precisely evaluated. We will employ GSM to calculate overlap functions and SFs of resonance states, as well as to pinpoint their internal physical mechanisms.

Ab initio no-core shell model (NCSM) is also considered for comparison, in which all nucleons are active and interact via a realistic interaction [41]. The basis of harmonic oscillator (HO) states is indeed suitable only for closed quantum system (CQS) [41], in which only bound valence shells are mainly occupied in the s.p. basis.

After a brief introduction to the theoretical frameworks of GSM and NCSM, we compare the results of calculated energy spectra and resonance widths of neutron-rich helium isotopes and their proton-rich isotones with experimental data. SFs and overlap functions of resonance states will be compared using both GSM and NCSM. Results allow to investigate the effects of continuum coupling in resonance states. A summary is provided afterwards.

II. METHOD.

The Gamow state, also known as complex-energy resonance state, was firstly proposed by George Gamow in 1932 to describe α decay [42]. By describing a nuclear state in the complex-energy plane, the theory of Gamow resonance state provides a natural definition of resonance state [42]. Resonance states lie above decay thresholds, so that they can decay via the emission of a nucleon, or of clusters such as deuteron, ^3He /triton, α particles, etc.

For a given GSM eigenstate, the eigenenergy of the many-body state can be written as [43],

$$\tilde{E} = E - i\Gamma/2, \quad (1)$$

where the real part E corresponds to the position of the resonance, while the imaginary part Γ is the resonance width, which is related to the lifetime of the state.

The Berggren completeness relation allows to include resonance states in a complete set of one-body states. It had been firstly formulated by Tore Berggren and its expression is as follows [26] :

$$\sum_n u_n(r)u_n(r') + \int_{L_+} u(k,r)u(k,r')dk = \delta(r-r'), \quad (2)$$

where $u_n(r)$ is a bound or resonance state and $u(k,r)$ is a scattering state belonging to the L_+ contour in the complex-momentum plane. The Berggren basis is indeed the extension of the real-energy Newton completeness relation to the complex plane [44]. Contrary to the Newton completeness relation, which only expands localized bound states, the Berggren basis can expand unbound resonance states. Within the Berggren representation, continuous states are located on the contour L_+ of the fourth quadrant of the complex plane, and the resonance states lying between the contour L_+ and the real-energy axis are included in the discrete sum of Eq. (2) along with bound states. Continuous states on the contour L_+ are discretized using the Gauss-Legendre method in order for the completeness relation of Eq. (2) to be used in numerical applications.

Due the presence of complex-energy states in the Berggren basis of Eq. (2), the Hamiltonian of GSM is represented therein by a complex symmetric matrix, which is diagonalized using the complex extension of the Jacobi-Davidson method [29]. Resonance states are identified in the complex-energy eigenspectrum of unbound states formed by both resonant and scattering eigenstates by using the overlap method [27, 29].

In the *ab-initio* NCSM, all nucleons in the A -body nuclear system are active, so that the NCSM Hamiltonian writes :

$$\hat{H} = \sum_{i<j} \frac{(p_i - p_j)^2}{2Am} + \hat{V}_{NN} + \dots \quad (3)$$

where m is the nucleon mass, \hat{V}_{NN} is the realistic two-body interaction, to which three-, four-, ... body forces can be added in principle. We will only use two-body interactions in this work.

In NCSM, the dimensionality of the matrix explodes as the number of nucleon increases, so that a truncation of the model space is typically required. In our calculations, the standard N_{max} truncation is used, i.e. the HO energy of basis Slater determinants is at most $N_{\text{max}} \hbar\omega$. The convergence of NCSM eigenenergies with respect to N_{max} can be found in Ref.[45, 46]. As the many-body Schrödinger equation of Eq. (3) is diagonalized using a finite number of HO basis states, whereby $N_{\text{max}} \leq 20$ is typical, its eigenstates are deeply bound independently of their eigenenergy value.

The overlap function $I_{\ell j}(r)$ is defined as:

$$\begin{aligned} I_{\ell j}(r) &= \langle \Psi_A^{JA} | \left[|\Psi_{A-1}^{JA-1}\rangle \otimes |r\ell j\rangle^{JA} \right] \rangle, \\ &= \frac{1}{\sqrt{2J_A+1}} \sum_i \langle \Psi_A^{JA} | |a_{n_i \ell j}^\dagger| |\Psi_{A-1}^{JA-1}\rangle u_{n_i}(r) \rangle, \end{aligned} \quad (4)$$

where $|\Psi_A^{JA}\rangle$ and $|\Psi_{A-1}^{JA-1}\rangle$ are the wave functions of the A and $A-1$ nuclear systems, respectively; ℓ and j are respectively the orbital and total angular momenta of the considered partial wave in $I_{\ell j}(r)$; $a_{n_i \ell j}^\dagger$ is the creation operator associated with the $|n_i \ell j\rangle$ state and is either the

n_i -th state of the HO basis (NCSM) or of the discretized Berggren basis (GSM); $u_{n_i}(r)$ represents the radial wave function of the $|n_i \ell j\rangle$ state. Overlap functions of Eq. (4) are independent of the used Berggren basis due to its completeness properties, contrary to NCSM, where overlap functions depend on N_{\max} .

SF is defined as being the norm of the radial overlap function $I_{\ell j}(r)$ of Eq. (4):

$$C^2S = \int I_{\ell j}(r)^2 dr, \quad (5)$$

where C^2S is a standard notation for SF. As the GSM framework makes use of complex-energy basis states, SFs are complex in general, contrary to the real-energy case. The imaginary parts of SFs can be interpreted as the uncertainty on real parts generated by the finite life-time of the nuclear system [27, 29]. From Eqs. (4,5), the complex effects of inter-nucleon correlations and continuum coupling on the asymptotic behavior of resonance states can be directly pointed out [20, 39].

III. RESULTS.

The purpose of this study is multifaceted. First, we investigate the energy spectrum and widths of resonance states of neutron-rich helium isotopes and isotones with GSM and NCSM. Second, we study how SFs and overlap functions are affected by threshold effects and coupling to the non-resonant continuum. We aim to outline the fundamental features and characteristics of resonance states using SFs and overlap functions.

We will use GSM in the core plus valence particle picture. The GSM Hamiltonian will then consist of a one-body finite depth Woods-Saxon (WS) potential mimicking the inert ^4He core and of a residual two-body interaction among valence nucleons. In the present work, we use for that matter the Gaussian-based Furutani, Horiuchi, and Tamagaki (FHT) residual two-body interaction, which is composed of central, spin-orbit, and tensor parts [47]. The Hamiltonian parameters and model space of Ref. [48] are adopted in the present work. The FHT interaction has been successfully used in the GSM to describe the properties of $A = 5 - 10$ light neutron-rich nuclei [33, 48], the mirror states in $^{16}\text{F}/^{16}\text{N}$ [49], and radiative capture reactions of $A = 6 - 8$ nuclei [50]. The Coulomb interaction is exactly included in the proton space. We will consider in this work weakly bound and resonance p -shell nuclei. All partial waves up to $l = 3$ are taken into account. As $d_{3/2}$ and $f_{7/2}, f_{5/2}$ partial waves bear a large centrifugal barrier, their effect on the asymptotic behavior of the wave function is negligible, so that they are expanded with a HO basis. We use the Berggren basis for the representation of $s_{1/2}, p_{3/2}, p_{1/2}, d_{5/2}$ partial waves, which form the most important part in nuclear wave function asymptotes. The $p_{3/2}$ and $p_{1/2}$ partial waves are discretized by 60 points along the contour L_+ ,

TABLE I. The calculated point-proton radius (r_p), point-neutron radius (r_n), and nuclear matter radius (r_m) of $^6, ^8\text{He}$ with GSM and NCSM methods, compared with experimental data [58–62].

^6He	r_p	r_n	r_m
NCSM	1.938	2.641	2.429
GSM	1.868	2.555	2.348
Exp	1.925(12) [58]	2.45(9) [58]	2.29(6) [58]
		2.47(10) [59]	2.30(7) [59]
		2.51(6) [60]	2.33(4) [60]
		2.61(3) [61]	2.48(3) [61]
		2.66(10) [62]	2.44(7) [62]
^8He	r_p	r_n	r_m
NCSM	1.819	2.570	2.404
GSM	1.904	2.725	2.545
Exp	1.807(28) [58]	2.73(9) [58]	2.53(7) [58]
		2.63(9) [59]	2.45(7) [59]
		2.68(5) [60]	2.49(4) [60]
		2.69(10) [62]	2.50(8) [62]

while the $s_{1/2}$ and $d_{5/2}$ partial wave are discretized by 30 points. The maximal momentum value for the contours is $k_{\max} = 4.0 \text{ fm}^{-1}$. In performed GSM calculations, three nucleons at most can occupy states in the non-resonant continuum. These parameters are sufficiently large to insure convergence for all the observables of interest.

In NCSM, we use the Daejeon16 two-body interaction, which is based on an SRG-transformed chiral N^3LO interaction [51]. It provides a good description of various observables in light nuclei without three-body forces and also generates rapid convergence for energy in *ab-initio* calculations [51]. The HO basis with a frequency of $\hbar\omega = 15 \text{ MeV}$ is utilized. The model space consists of an $N\hbar\omega$ space [52], where $N \leq N_{\max}$. We attempt to perform computations in large model spaces in order to achieve convergent results. However, due to limited computing power, maximal truncations are $N_{\max} = 12$ for $A = 5$ and 6 nuclei, and $N_{\max} = 10$ for $A = 7$ and 8 nuclei. The results of extrapolating the energy spectrum to infinite-size model spaces [46, 53] are shown in Fig. 1.

The energies of the low-lying states of the $^5\text{--}^8\text{He}$ isotopes and their isotones in ^5Li , ^6Be , ^7B , and ^8C nuclei are calculated in NCSM and GSM. Results are displayed in Fig. 1, along with experimental data [54–57]. As one considers mirror nuclei, it is interesting to compare their energies and decay widths, which would be otherwise identical in the absence of the Coulomb force. Indeed, significant differences appear due to the presence of the Coulomb Hamiltonian among valence protons in helium isotones. A good reproduction of these isotonic states is obtained in our GSM calculations. Discrepancy with respect to experiment is of a few hundreds of keV when using the FHT two-body interaction. On the one hand, the calculated ground-state energies of helium isotopes

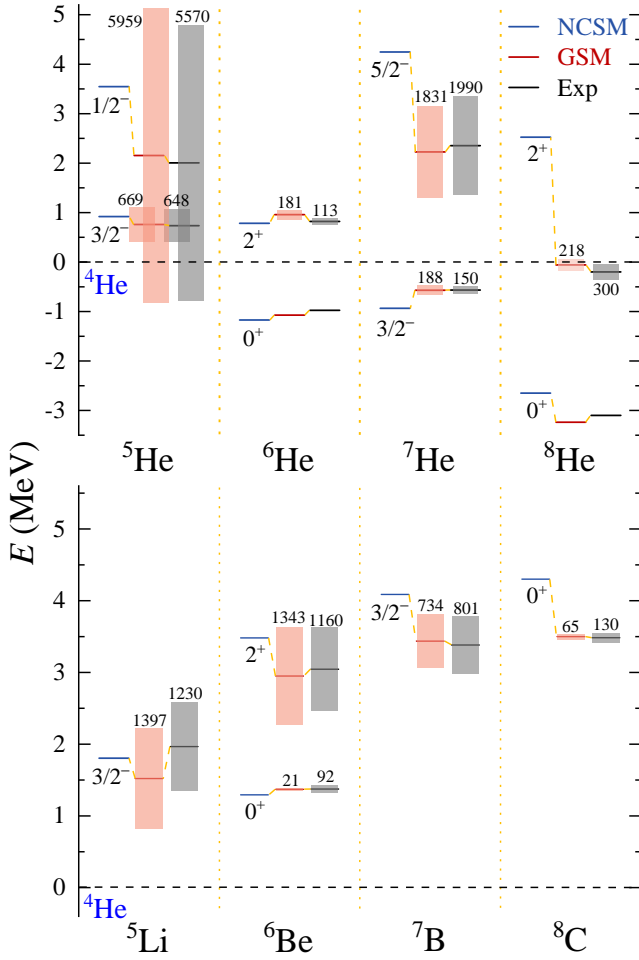


FIG. 1. Low-lying spectra (in MeV) and widths (in keV) of the isotopes of ${}^5\text{--}8\text{He}$ (upper), and the isotones of ${}^5\text{Li}$, ${}^6\text{Be}$, ${}^7\text{B}$, and ${}^8\text{C}$ (lower). The calculations illustrated by blue and red lines are provided by NCSM and GSM, respectively, and the experimental data are taken from Ref. [54–57]. Ground-state energies are given with respect to that of ${}^4\text{He}$. Shaded areas represent the resonance width in the GSM calculations and experimental data, with their explicit values written above.

and isotones using NCSM and GSM are both close to experimental data. However, the calculated excitation energies of excited states in NCSM, on the other hand, are generally higher than those of GSM and experimental data. The ${}^6,8\text{He}$ isotopes exhibit neutron halos around the ${}^4\text{He}$ -like core, which makes a precision measurement of the charge radii essential for probing the many-body wave function of the neutron halos [63]. We also calculated the proton-point, neutron-point, and matter radii of ${}^6,8\text{He}$ with both NCSM and GSM. Results are presented in Table. I, along with experimental data. Both GSM and NCSM calculations yield good agreement with experimental data.

The GSM decay widths of the neutron-rich helium isotopes agree well with experimental data. As the Coulomb

barrier is low in light nuclei, unbound states of sizable width can form at the proton drip line. GSM accurately reproduces the proton-emission widths of the resonance states of helium isotones. The difference between calculated and experimental widths is indeed smaller than 200 keV. According to our GSM calculations, ${}^5\text{He}(1/2^-)$ is a broad ($\Gamma = 5959$ keV) resonance, as well as the ${}^7\text{He}(5/2^-)$ excited state ($\Gamma = 1831$ keV), values which are both consistent with experimental data, 5570 and 1990 keV for ${}^5\text{He}(1/2^-)$ and ${}^7\text{He}(5/2^-)$ [55], respectively.

The NCSM is diagonalized using a basis of HO states, implying that the nucleus is viewed as a CQS. While such an assumption is justified for well-bound nuclei, it can no longer be applied to unbound states. Weakly bound and unbound states bear a low-lying single-nucleon emission threshold and a large surface density space dispersion, due to a strong coupling to scattering states. It can then be expected that GSM will be better at describing resonance state features than NCSM.

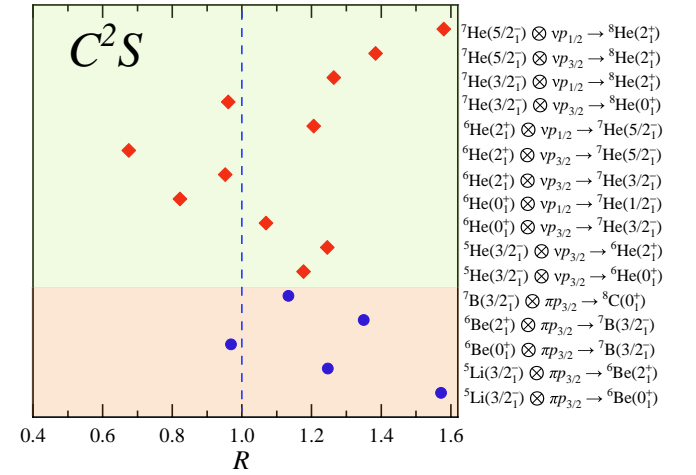


FIG. 2. C^2S values calculated with NCSM and GSM. Points represent the ratio of the GSM results to the NCSM results, which is defined as R . Red diamonds correspond to the C^2S values of neutron, while blue circles are related to the C^2S values of proton (see right side for specific reaction channels). The blue line pinpoints the $R = 1$ value. SF calculations are restricted to the $p_{3/2}$ and $p_{1/2}$ partial waves only.

SF is used as a predictive tool for detailed nuclear structure [22, 64, 65], and studies have shown that scattering continuum is critical for states near particle-emission threshold [22, 66]. To further investigate the properties of resonance states, especially the effects of continuum coupling, we calculated the overlap functions and SFs (C^2S in this paper) of the associated resonance states using NCSM and GSM.

The convergence of C^2S is slower as model spaces increase in dimension compared to energy in NCSM calculations. Added to that, exponential extrapolation of C^2S cannot be utilized as for eigenstate energy. Consequently, it is necessary to consider the C^2S and overlap functions

provided by the largest NCSM model space for comparison with GSM calculations. In order to investigate the differences between GSM and NCSM calculations and to demonstrate the continuum coupling effects, the ratio of GSM to NCSM results is studied, which is denoted as R (Imaginary parts are not considered as they cannot be evaluated in NCSM).

C^2S values involving $p_{3/2}$ and $p_{1/2}$ partial waves in He, Li, Be, B, and C isotopes bearing $A = 6 - 8$ nucleons are calculated and results presented in Fig. 2. Small SFs, i.e. for which $\text{Re}(C^2S) < 0.1$, are not displayed. Calculated SFs are listed in Tabs. II and III. **Even though SF is a well-defined theoretical concept [67], it is model-dependent [68] and can not be observed directly. The experimental extraction of SF requires the use of the distorted-wave Born approximation (DWBA) [69] or eikonal reaction theory [70]. In transfer reaction, SF can be obtained by fitting the angular distributions to the data points around resonance peaks in DWBA [69]. Whereas, in knockout reactions, SF is derived from the ratio of experimental and theoretical cross-sections [70].** Experimental data provide a SF for ${}^6\text{He}(0_1^+) \otimes \nu p_{3/2} \rightarrow {}^7\text{He}(3/2_1^-)$ of 0.512(18) [71], which is close to our GSM and NCSM calculations, giving 0.487 and 0.455, respectively.

The results of GSM and NCSM differ significantly if the R -value departs from the blue line. One can see that $R \simeq 1$ in the SFs associated to ${}^6\text{He}(0_1^+) \otimes \nu p_{3/2} \rightarrow {}^7\text{He}(3/2_1^-)$, ${}^6\text{He}(2_1^+) \otimes \nu p_{3/2} \rightarrow {}^7\text{He}(3/2_1^-)$, and ${}^7\text{He}(3/2_1^-) \otimes \nu p_{3/2} \rightarrow {}^8\text{He}(0_1^+)$. Indeed, the correlated nucleon states of ${}^{6-8}\text{He}$ are bound or narrow resonance states in this case, so that continuum coupling is reduced. Moreover, in the vast majority of cases, one obtains $|R - 1| \sim 0.2 - 0.6$, thus pointing out strong continuum coupling effects. When the $A - 1$ or/and A nuclear states involved in the SF calculation are broad resonances, coupling to the continuum is prominent. For example, $|R - 1| > 0.2$ when the $A - 1$ -nucleus is ${}^5\text{Li}$ (g.s.) or the A -nucleus is ${}^7\text{He}(5/2_1^-)$, which are broad resonances. One of the largest difference between the results of NCSM and GSM calculations is indeed obtained for the reaction ${}^5\text{Li}(3/2_1^-) \otimes \pi p_{3/2} \rightarrow {}^6\text{Be}(0_1^+)$, where $R \simeq 1.6$. Similarly, the R value of the reactions ${}^6\text{He}(2_1^+) \otimes \nu p_{3/2} \rightarrow {}^7\text{He}(5/2_1^-)$ and ${}^7\text{He}(5/2_1^-) \otimes \nu p_{1/2} \rightarrow {}^8\text{He}(2_1^+)$ is also not close to 1. However, there are exceptions to this rule, with, for example, the reaction ${}^6\text{Be}(0_1^+) \otimes \nu p_{3/2} \rightarrow {}^7\text{B}(3/2_1^-)$. Even though a resonance width of about 700 keV is obtained for the unbound ${}^7\text{B}(\text{g.s.})$, while ${}^6\text{Be}(\text{g.s.})$ is also unbound, one has $R \simeq 1$ in this case. One can note that a strong continuum coupling does not generate either an increase or a decrease of R , as both the occurrences $R < 1$ and $R > 1$ occur when broad resonances are present (see Fig. 2). Illustrations of the strong influence of continuum coupling on spectroscopic observables in unbound systems can also be found in Ref. [72].

TABLE II. C^2S values issued from NCSM and GSM calculations for $p_{3/2}$ partial wave. R is the ratio between GSM and NCSM C^2S values. One uses a NCSM model space of $(N_{\text{max}}^{A-1}, N_{\text{max}}^A) = (12, 12)$ for $A = 5$ and 6 nuclei, and $(N_{\text{max}}^{A-1}, N_{\text{max}}^A) = (10, 10)$ for $A = 7$ and 8 nuclei. Parent and daughter nuclei are denoted by $A - 1$ and A , respectively.

				$C^2S(p_{3/2})$		
$A - 1$	$(J^\pi)_{A-1}$	A	$(J^\pi)_A$	GSM	NCSM	R
${}^5\text{He}$	$3/2_1^-$	${}^6\text{He}$	0_1^+	$1.850 - 0.747$	1.572	1.177
	$3/2_1^-$		2_1^+	$1.855 + i0.096$	1.490	1.245
	$1/2_1^-$		2_1^+	$0.138 - i0.015$	0.094	1.468
${}^6\text{He}$	0_1^+	${}^7\text{He}$	$3/2_1^-$	$0.487 + i0.101$	0.455	1.069
	2_1^+		$3/2_1^-$	$1.865 - i0.446$	1.931	0.966
	2_1^+		$5/2_1^-$	$0.140 - i0.070$	0.208	0.675
${}^7\text{He}$	$3/2_1^-$	${}^8\text{He}$	0_1^+	$3.222 - i0.664$	3.384	0.952
	$5/2_1^-$		2_1^+	$2.386 + i0.788$	1.724	1.384
${}^5\text{Li}$	$3/2_1^-$	${}^6\text{Be}$	0_1^+	$2.421 - i0.353$	1.540	1.572
	$3/2_1^-$		2_1^+	$1.822 + i0.022$	1.461	1.247
${}^6\text{Be}$	0_1^+	${}^7\text{B}$	$3/2_1^-$	$0.436 + i0.012$	0.450	0.969
	2_1^+			$2.573 - i0.074$	1.906	1.350
${}^7\text{B}$	$3/2_1^-$	${}^8\text{C}$	0_1^+	$3.788 + i0.112$	3.340	1.134

TABLE III. Similar to Tab. II, but for C^2S of $p_{1/2}$ partial wave.

				$C^2S(p_{1/2})$		
$A - 1$	$(J^\pi)_{A-1}$	A	$(J^\pi)_A$	GSM	NCSM	R
${}^5\text{He}$	$1/2_1^-$	${}^6\text{He}$	0_1^+	$0.246 - i0.150$	0.104	2.363
${}^6\text{He}$	0_1^+	${}^7\text{He}$	$1/2_1^-$	$0.585 - i0.023$	0.712	0.822
	2_1^+		$5/2_1^-$	$0.821 - i0.005$	0.681	1.206
${}^7\text{He}$	$3/2_1^-$	${}^8\text{He}$	2_1^+	$0.996 - i0.127$	0.788	1.264

Continuum coupling modifies both SFs and overlap functions involving resonance states. As a consequence, we will study the overlap functions that correspond to the C^2S values of Fig. 2. Overlap functions provide details on the nuclear structure both inside the nucleus and in the asymptotic zone [19, 65]. They are illustrated in Figs. 3, 4, and 5, where both real and imaginary parts are shown. We only considered overlap functions involving the $p_{3/2}$ partial wave because the latter is dominant in the studied nuclei. As the centrifugal barrier is small in the $\ell = 1$ partial wave, one can expect the A or $A - 1$ nucleus, and hence the overlap function, to be extended in the asymptotic zone with GSM. This indeed the case for all the overlap functions obtained in GSM, which always lie above NCSM overlap functions in the asymptotic region (see Figs. 3, 4, and 5). This phenomenon is even more pronounced when the state of the A or $A - 1$ nucleus lies beyond particle-emission threshold. Indeed, due to the unbound character of the involved wave function, the overlap function can present both negative values in its

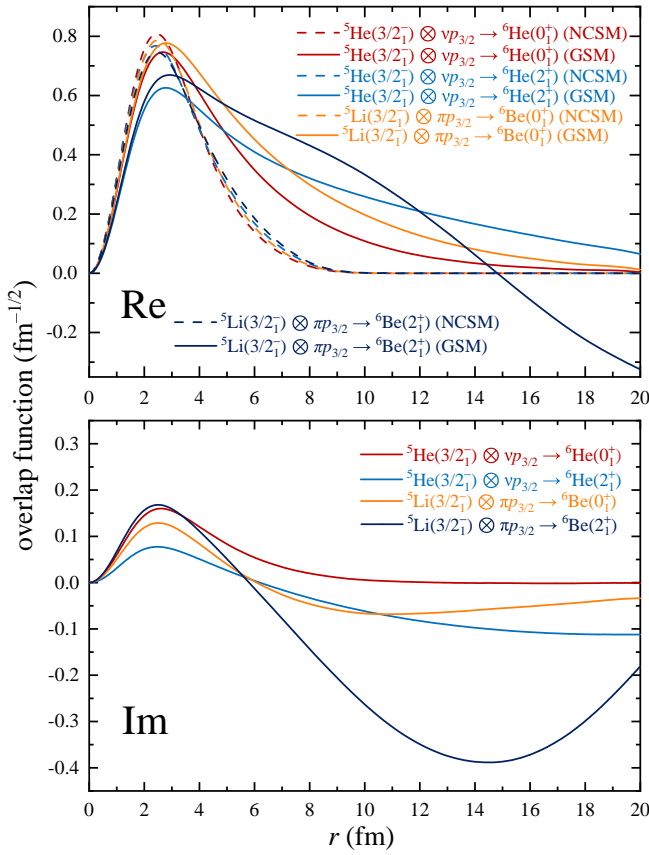


FIG. 3. Calculated the overlap functions of $p_{3/2}$ partial wave in $|A=5\rangle \otimes p_{3/2} \rightarrow |A=6\rangle$ systems with NCSM (dashed lines) and GSM (solid lines). The real part for NCSM and GSM are shown in the upper panel, and the imaginary part of GSM is shown in the lower panel.

real part and large imaginary parts in modulus, whereby an oscillation pattern develops (see the overlap functions of the reaction ${}^5\text{Li}(3/2^-) \otimes \nu p_{3/2} \rightarrow {}^6\text{Be}(2_1^+)$ in Fig. 3 and ${}^6\text{Be}(0_1^+) \otimes \pi p_{3/2} \rightarrow {}^7\text{B}(3/2^-)$, ${}^6\text{He}(0_1^+) \otimes \nu p_{3/2} \rightarrow {}^7\text{He}(3/2^-)$ in Fig. 4). Conversely, the overlap functions obtained in the NCSM are large inside the nucleus and rapidly decrease to zero outside the nucleus, which is caused by the localized character of the used HO basis states therein.

Nuclei of drip-line regions typically exhibit significant isospin-symmetry breaking, such as large mirror energy difference of mirror states [73, 74] and abnormal isobaric multiplet mass equation [74]. GSM overlap function show that there is a large isospin-symmetry breaking in investigated mirror partners. For instance, the asymptotic behavior of the nuclei in the reaction ${}^5\text{He}(3/2^-) \otimes \nu p_{3/2} \rightarrow {}^6\text{He}(2_1^+)$ and in its mirror case, as shown in Fig. 3, show noticeable differences. Moreover, the values of the overlap function associated to the reaction ${}^5\text{He}(3/2^-) \otimes \nu p_{3/2} \rightarrow {}^6\text{He}(2_1^+)$ is smaller than that of its mirror inside of the nucleus. This situation reverses outside of the nucleus, whereby the overlap function of

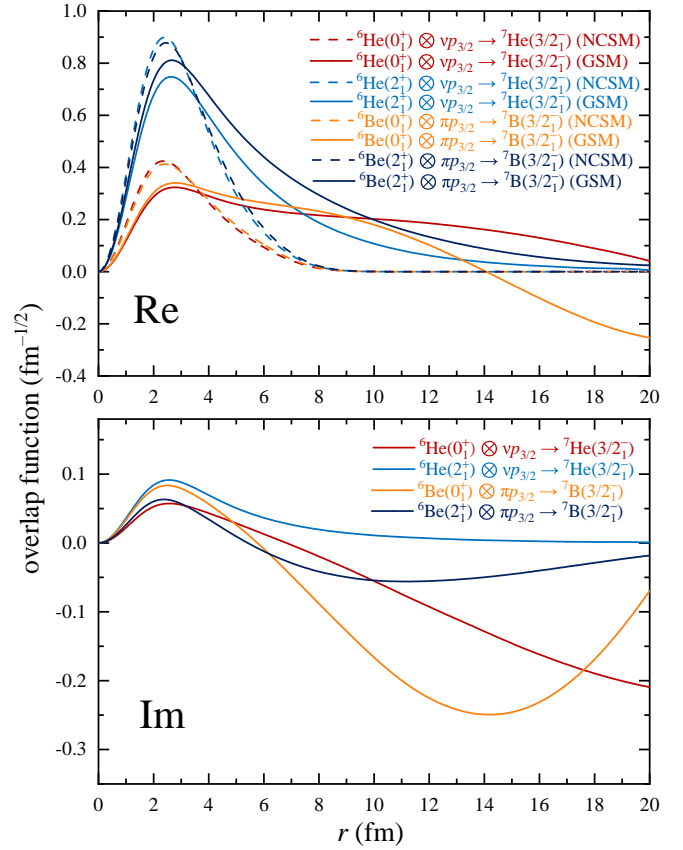


FIG. 4. Similar to Fig. 3, but for overlap functions of the $|A=6\rangle \otimes p_{3/2} \rightarrow |A=7\rangle$ systems.

the mirror reaction ${}^5\text{Li}(3/2^-) \otimes \pi p_{3/2} \rightarrow {}^6\text{Be}(2_1^+)$ rapidly decreases therein and can become negative. The imaginary parts of overlap functions are also larger in the mirror reaction of the proton-rich side, due to the larger widths present therein in the A or $A-1$ nucleus. A similar phenomenon of isospin-symmetry breaking can also be seen in the GSM calculations illustrated in Figs. 4 and 5. On the contrary, the difference between mirror nuclei is barely discernible in NCSM overlap functions, even though the Coulomb interaction is considered exactly in NCSM (see Figs. 3, 4, and 5). Thus, the influence of continuum coupling in the observables involving drip-line nuclei is more significant for isospin-symmetry breaking than the simple inclusion of the Coulomb force in the many-body Hamiltonian. A large number of HO states might be able to generate isospin-symmetry breaking in NCSM results, but the dimensionality of associated NCSM model spaces would be enormous, far beyond the capabilities of current supercomputers, and that due to the slow convergence of SFs and overlap functions with increasing N_{max} . In fact, only GSM can depict continuum coupling properly via the explicit use of scattering states in the Berggren basis. While the effects of the non-resonant continuum can be mimicked by a few HO basis states in energy spectra, this is not the case for

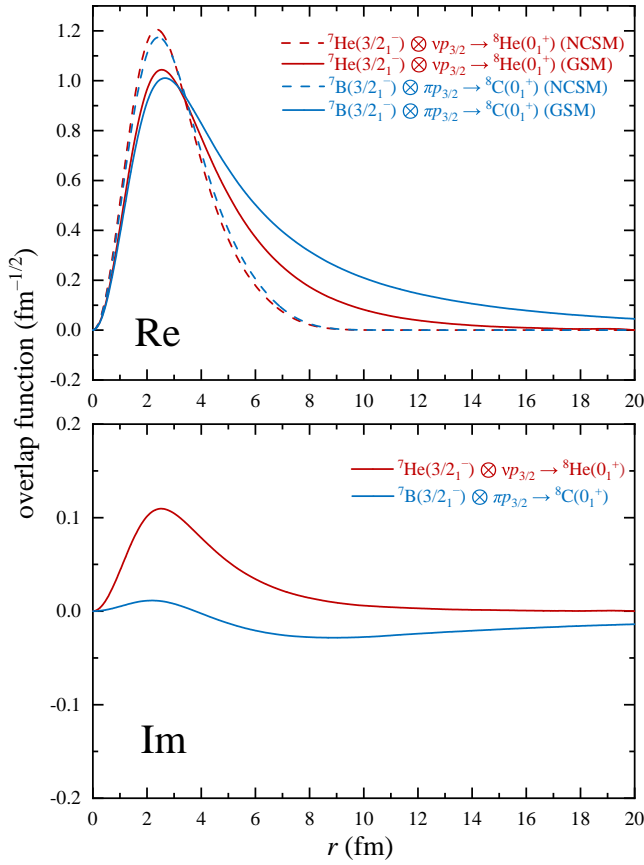


FIG. 5. Similar to Fig. 3, but for overlap functions of the $|A=7\rangle \otimes p_{3/2} \rightarrow |A=8\rangle$ systems.

observables depending on the structure of nuclear wave functions in the asymptotic region, such as SFs and overlap functions.

Only the C^2S value of ${}^6\text{He}(0_1^+) \otimes \nu p_{3/2} \rightarrow {}^7\text{He}(3/2_1^-)$ has been measured experimentally. In Fig. 6, we present calculated overlap function and C^2S using both NCSM and GSM, along with theoretical results from variational Monte Carlo (VMC) and Green's function Monte Carlo (GFMC) [75], as well as experimental C^2S data [71, 76, 77]. Results indicate that the overlap functions calculated with GSM and GFMC are more extended than those from NCSM and VMC, and that the GSM overlap function exhibits the resonance character of ${}^7\text{He}(3/2_1^-)$ state. However, the C^2S values obtained from VMC and GFMC are slightly larger than those from NCSM and GSM. Nevertheless, all calculated C^2S values are in agreement with experimental data.

Furthermore, we also performed NCSM calculations using chiral N^3LO potential with $\lambda = 2.0$ in SRG and chiral N^2LO potential, and the resulting C^2S values of ${}^6\text{He}(0_1^+) \otimes \nu p_{3/2} \rightarrow {}^7\text{He}(3/2_1^-)$ are close to each other due to the localization of the many-body wave function in NCSM calculation. GSM calculations have also been performed using a Minnesota interaction with different strengths. Results indicate that the calculated C^2S val-

ues depend on the one-neutron separation energy (S_n) of ${}^7\text{He}(3/2_1^-)$ state, and that C^2S is close to the results obtained with the FHT interaction when the corresponding S_n is close as well. Therefore, due to near-threshold effects, C^2S is sensitive to S_n .

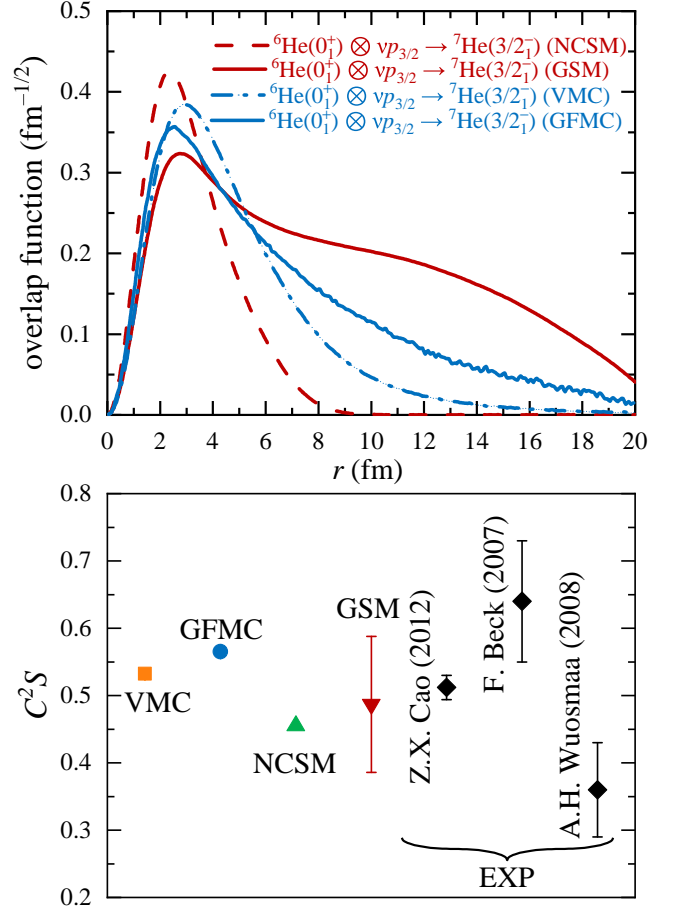


FIG. 6. Comparison of the overlap function and C^2S of ${}^6\text{He}(0_1^+) \otimes \nu p_{3/2} \rightarrow {}^7\text{He}(3/2_1^-)$ using NCSM and GSM, along with VMC and GFMC calculations [75], as well as experimental data [71, 76, 77].

IV. SUMMARY.

The study of unbound resonance states is of great significance for the comprehension of the properties of atomic nuclei at drip-lines. In this paper, we investigated neutron-rich nuclei and their proton-rich mirrors at neutron and proton drip-lines using the GSM and NCSM. The importance of continuum coupling could be precisely assessed by comparing nuclear energies, widths, as well as SFs and overlap functions.

First, we calculated the energy spectrum of the helium isotopes and isotones with GSM and NCSM, where the decay widths of resonance states are also provided from GSM calculations. We utilized a phenomenologi-

cal Hamiltonian in GSM, in the core plus valence particle picture, with a WS potential mimicking the ^4He and the FHT two-body interaction as residual interaction among valence nucleons. The Daejeon16 two-body realistic interaction, based on an SRG-transformed chiral N^3LO interaction, is used in the NCSM Hamiltonian. The Coulomb force is exactly taken into account in both NCSM and GSM Hamiltonians.

GSM fairly describes the low-lying energy spectrum and resonance widths of $^5\text{--}^8\text{He}$ isotopes and ^5Li , ^6Be , ^7B , and ^8C isotones. Compared to NCSM results, we could already see that continuum effects play an essential role in the description of weakly bound and resonance states at spectrum level. The asymptotic behavior of resonance states could be precisely investigated in nuclear many-body wave functions from the calculation of SFs and overlap functions. We have indeed demonstrated the effect of continuum coupling in SFs and overlap functions of drip-line helium isotopes and isotones. Comparisons of calculated SFs in GSM and NCSM show that the continuum coupling has a significant effect on SFs and overlap functions. Indeed, continuum coupling induces changes in the SFs of GSM and NCSM, as the ratio of SFs in GSM compared to those of NCSM can be both smaller or larger than 1, where relative differences can be as large as 60%. Added to that, the overlap functions obtained in GSM are all extended in space, whereas they are localized in NCSM. One could also notice the large imaginary parts present in the SFs and overlap functions of GSM when unbound states are involved. They provide information

about the uncertainty of the real parts of SFs and overlap functions in GSM, which is generated by the finite life-time of present resonance states. One could also see an oscillation pattern develop in GSM overlap functions when broad resonances are considered. Isospin-symmetry breaking is also clearly seen in GSM, as SFs and overlap functions of mirror nuclei vary significantly, which is generated by the Coulomb Hamiltonian in the asymptotic region. These features cannot be seen in NCSM overlap functions, even though the Coulomb force is included.

This study has then proved that continuum coupling and a proper depiction of many-body nuclear wave function asymptotes is prominent for the comprehension of drip-line nuclei. This provides the possibility to precisely study ANC's in drip-line nuclei in the future, which are important for the calculation of capture cross sections at astrophysical energies, for example.

Acknowledgments. This work has been supported by the National Natural Science Foundation of China under Grant Nos. 12205340, 12175281, and 11975282; the Gansu Natural Science Foundation under Grant No. 22JR5RA123; the Strategic Priority Research Program of Chinese Academy of Sciences under Grant No. XDB34000000; the Key Research Program of the Chinese Academy of Sciences under Grant No. XDPB15; the State Key Laboratory of Nuclear Physics and Technology, Peking University under Grant No. NPT2020KFY13. This research was made possible by using the computing resources of Gansu Advanced Computing Center.

-
- [1] N. Smirnova, B. Bally, K. Heyde, F. Nowacki, and K. Sieja, *Phys. Lett. B* **686**, 109 (2010).
 - [2] G. Hagen, M. Hjorth-Jensen, G. R. Jansen, R. Machleidt, and T. Papenbrock, *Phys. Rev. Lett.* **109**, 032502 (2012).
 - [3] A. S. Jensen, K. Riisager, D. V. Fedorov, and E. Garrido, *Rev. Mod. Phys.* **76**, 215 (2004).
 - [4] J. Bonnard, S. M. Lenzi, and A. P. Zuker, *Phys. Rev. Lett.* **116**, 212501 (2016).
 - [5] M. Pfützner, M. Karny, L. V. Grigorenko, and K. Riisager, *Rev. Mod. Phys.* **84**, 567 (2012).
 - [6] C. Detraz, M. Epherre, D. Guillemaud, P. Hansen, B. Jonson, R. Klapisch, M. Langevin, S. Mattsson, F. Naulin, G. Nyman, A. Poskanzer, H. Ravn, M. de Saint-Simon, K. Takahashi, C. Thibault, and F. Touchard, *Phys. Lett. B* **94**, 307 (1980).
 - [7] H. Koura and S. Chiba, *Energy Procedia* **71**, 228 (2015), the Fourth International Symposium on Innovative Nuclear Energy Systems, INES-4.
 - [8] R. E. Azuma, L. C. Carraz, P. G. Hansen, B. Jonson, K. L. Kratz, S. Mattsson, G. Nyman, H. Ohm, H. L. Ravn, A. Schröder, and W. Ziegert, *Phys. Rev. Lett.* **43**, 1652 (1979).
 - [9] F. M. Marqués, M. Labiche, N. A. Orr, J. C. Angélique, L. Axelsson, B. Benoit, U. C. Bergmann, M. J. G. Borge, W. N. Catford, S. P. G. Chappell, N. M. Clarke, G. Costa, N. Curtis, A. D'Arrigo, E. d. G. Brennand, F. d. O. Santos, O. Dorvaux, G. Fazio, M. Freer, B. R. Fulton, G. Giardina, S. Grévy, D. Guillemaud-Mueller, F. Hanappe, B. Heusch, B. Jonson, C. L. Brun, S. Leenhardt, M. Lewitowicz, M. J. López, K. Markenroth, A. C. Mueller, T. Nilsson, A. Ninane, G. Nyman, I. Piqueras, K. Riisager, M. G. Saint Laurent, F. Sarazin, S. M. Singer, O. Sorlin, and L. Stuttgé, *Phys. Rev. C* **64**, 061301 (2001).
 - [10] D. Baye and E. Tursunov, *Phys. Lett. B* **696**, 464 (2011).
 - [11] K. J. Cook, T. Nakamura, Y. Kondo, K. Hagino, K. Ogata, A. T. Saito, N. L. Achouri, T. Aumann, H. Baba, F. Delaunay, Q. Deshayes, P. Doornenbal, N. Fukuda, J. Gibelin, J. W. Hwang, N. Inabe, T. Isobe, D. Kameda, D. Kanno, S. Kim, N. Kobayashi, T. Kobayashi, T. Kubo, S. Leblond, J. Lee, F. M. Marqués, R. Minakata, T. Motobayashi, K. Muto, T. Murakami, D. Murai, T. Nakashima, N. Nakatsuka, A. Navin, S. Nishi, S. Ogoshi, N. A. Orr, H. Otsu, H. Sato, Y. Satou, Y. Shimizu, H. Suzuki, K. Takahashi, H. Takeda, S. Takeuchi, R. Tanaka, Y. Togano, J. Tsubota, A. G. Tuff, M. Vandebrouck, and K. Yoneda, *Phys. Rev. Lett.* **124**, 212503 (2020).
 - [12] N. Kobayashi, T. Nakamura, Y. Kondo, J. A. Tostevin, Y. Utsuno, N. Aoi, H. Baba, R. Barthelemy, M. A. Famiano, N. Fukuda, N. Inabe, M. Ishihara, R. Kanungo, S. Kim, T. Kubo, G. S. Lee, H. S. Lee, M. Matsushita, T. Motobayashi, T. Ohnishi, N. A. Orr, H. Otsu, T. Otsuka, T. Sako, H. Sakurai, Y. Satou, T. Sumikama,

- H. Takeda, S. Takeuchi, R. Tanaka, Y. Togano, and K. Yoneda, *Phys. Rev. Lett.* **112**, 242501 (2014).
- [13] R. Id Betan, R. J. Liotta, N. Sandulescu, and T. Vertse, *Phys. Rev. Lett.* **89**, 042501 (2002).
- [14] V. Girard-Alcindor, A. Mercenne, I. Stefan, F. de Oliveira Santos, N. Michel, M. Płoszajczak, M. Assié, A. Lemasson, E. Clément, F. Flavigny, A. Matta, D. Ramos, M. Rejmund, J. Dudouet, D. Ackermann, P. Adsley, M. Assunção, B. Bastin, D. Beaumel, G. Benzoni, R. Borcea, A. J. Boston, D. Brugnara, L. Cáceres, B. Cederwall, I. Celikovic, V. Chudoba, M. Ciemala, J. Collado, F. C. L. Crespi, G. D'Agata, G. De France, F. Delaunay, C. Diget, C. Domingo-Pardo, J. Eberth, C. Fougères, S. Franchoo, F. Galtarossa, A. Georgiadou, J. Gibelin, S. Giraud, V. González, N. Goyal, A. Gottardo, J. Goupil, S. Grévy, V. Guimaraes, F. Hammache, L. J. Harkness-Brennan, H. Hess, N. Jovančević, D. S. Judson Oliver, O. Kamalou, A. Kamenyero, J. Kiener, W. Korten, S. Koyama, M. Labiche, L. Lalanne, V. Lapoux, S. Leblond, A. Lefevre, C. Lenain, S. Leoni, H. Li, A. Lopez-Martens, A. Maj, I. Matea, R. Menegazzo, D. Mengoni, A. Meyer, B. Million, B. Monteagudo, P. Morfouace, J. Mrazek, M. Niikura, J. Piot, Z. Podolyak, C. Portail, A. Pullia, B. Quintana, F. Recchia, P. Reiter, K. Rezynekina, T. Roger, J. S. Rojo, F. Rotaru, M. D. Salsac, A. M. Sánchez Benítez, E. Sanchis, M. Şenyigit, N. de Séréville, M. Siciliano, J. Simpson, D. Sohler, O. Sorlin, M. Stanoiu, C. Stodel, D. Suzuki, C. Theisen, D. Thisse, J. C. Thomas, P. Ujic, J. J. Valiente-Dobón, and M. Zielińska, *Phys. Rev. C* **105**, L051301 (2022).
- [15] R. Id Betan, R. J. Liotta, N. Sandulescu, T. Vertse, and R. Wyss, *Phys. Rev. C* **72**, 054322 (2005).
- [16] N. Michel, W. Nazarewicz, M. Płoszajczak, and J. Okołowicz, *Phys. Rev. C* **67**, 054311 (2003).
- [17] N. Michel, J. G. Li, F. R. Xu, and W. Zuo, *Phys. Rev. C* **100**, 064303 (2019).
- [18] Y. Jin, C. Y. Niu, K. W. Brown, Z. H. Li, H. Hua, A. K. Anthony, J. Barney, R. J. Charity, J. Crosby, D. Dell'Aquila, J. M. Elson, J. Estee, M. Ghazali, G. Jhang, J. G. Li, W. G. Lynch, N. Michel, L. G. Sobotka, S. Sweany, F. C. E. Teh, A. Thomas, C. Y. Tsang, M. B. Tsang, S. M. Wang, H. Y. Wu, C. X. Yuan, and K. Zhu, *Phys. Rev. Lett.* **127**, 262502 (2021).
- [19] J. Okołowicz, N. Michel, W. Nazarewicz, and M. Płoszajczak, *Phys. Rev. C* **85**, 064320 (2012).
- [20] N. Michel, W. Nazarewicz, and M. Płoszajczak, *Phys. Rev. C* **75**, 031301 (2007).
- [21] N. Michel, W. Nazarewicz, and M. Płoszajczak, *Phys. Rev. C* **82**, 044315 (2010).
- [22] M. R. Xie, J. G. Li, N. Michel, H. H. Li, S. T. Wang, H. J. Ong, and W. Zuo, *Phys. Lett. B*, 137800 (2023).
- [23] J. Okołowicz, M. Płoszajczak, and I. Rotter, *Phys. Rep.* **374**, 271 (2003).
- [24] B. Blank and M. Płoszajczak, *Rep. Prog. Phys.* **71**, 046301 (2008).
- [25] J. Rotureau, J. Okołowicz, and M. Płoszajczak, *Phys. Rev. Lett.* **95**, 042503 (2005).
- [26] T. Berggren, *Nucl. Phys. A* **109**, 265 (1968).
- [27] N. Michel, W. Nazarewicz, M. Płoszajczak, and T. Vertse, *J. Phys. G: Nucl. Part. Phys.* **36**, 013101 (2009).
- [28] J. G. Li, Y. Z. Ma, N. Michel, B. S. Hu, Z. H. Sun, W. Zuo, and F. R. Xu, *Physics* **3**, 977 (2021).
- [29] N. Michel and M. Płoszajczak, *Gamow Shell Model, The Unified Theory of Nuclear Structure and Reactions, Lecture Notes in Physics*, Vol. 983 (Springer, Berlin, 2021).
- [30] J. G. Li, N. Michel, B. S. Hu, W. Zuo, and F. R. Xu, *Phys. Rev. C* **100**, 054313 (2019).
- [31] J. G. Li, N. Michel, W. Zuo, and F. R. Xu, *Phys. Rev. C* **103**, 034305 (2021).
- [32] N. Michel, J. G. Li, F. R. Xu, and W. Zuo, *Phys. Rev. C* **103**, 044319 (2021).
- [33] H. H. Li, J. G. Li, N. Michel, and W. Zuo, *Phys. Rev. C* **104**, L061306 (2021).
- [34] M. B. Tsang, J. Lee, and W. G. Lynch, *Phys. Rev. Lett.* **95**, 222501 (2005).
- [35] P. Hansen and J. Tostevin, *Ann. Rev. Nucl. Part. Sci.* **53**, 219 (2003).
- [36] J. Li, C. A. Bertulani, and F. Xu, *Phys. Rev. C* **105**, 024613 (2022).
- [37] J. A. Tostevin and A. Gade, *Phys. Rev. C* **90**, 057602 (2014).
- [38] J. A. Tostevin and A. Gade, *Phys. Rev. C* **103**, 054610 (2021).
- [39] J. Wylie, J. Okołowicz, W. Nazarewicz, M. Płoszajczak, S. M. Wang, X. Mao, and N. Michel, *Phys. Rev. C* **104**, L061301 (2021).
- [40] N. Michel, W. Nazarewicz, and M. Płoszajczak, *Phys. Rev. C* **70**, 064313 (2004).
- [41] B. R. Barrett, P. Navrátil, and J. P. Vary, *Prog. Part. Nucl. Phys.* **69**, 131 (2013).
- [42] A. J. F. Siegert, *Phys. Rev.* **56**, 750 (1939).
- [43] N. Michel, W. Nazarewicz, M. Płoszajczak, and K. Benaceur, *Phys. Rev. Lett.* **89**, 042502 (2002).
- [44] R. G. Newton, *Scattering theory of waves and particles* (Springer Berlin, Heidelberg, 2013).
- [45] P. Maris, J. P. Vary, and A. M. Shirokov, *Phys. Rev. C* **79**, 014308 (2009).
- [46] G. A. Negoita, J. P. Vary, G. R. Luecke, P. Maris, A. M. Shirokov, I. J. Shin, Y. Kim, E. G. Ng, C. Yang, M. Lockner, and G. M. Prabhu, *Phys. Rev. C* **99**, 054308 (2019).
- [47] H. Furutani, H. Horiuchi, and R. Tamagaki, *Prog. Theo. Phys.* **62**, 981 (1979).
- [48] Y. Jaganathen, R. M. I. Betan, N. Michel, W. Nazarewicz, and M. Płoszajczak, *Phys. Rev. C* **96**, 054316 (2017).
- [49] N. Michel, J. G. Li, L. H. Ru, and W. Zuo, *Phys. Rev. C* **106**, L011301 (2022).
- [50] K. Fosse, N. Michel, M. Płoszajczak, Y. Jaganathen, and R. M. Id Betan, *Phys. Rev. C* **91**, 034609 (2015).
- [51] A. Shirokov, I. Shin, Y. Kim, M. Sosonkina, P. Maris, and J. Vary, *Phys. Lett. B* **761**, 87 (2016).
- [52] J. Vary, O. Atramantov, B. Barrett, M. Hasan, A. Hayes, R. Lloyd, A. Mazur, P. Navrátil, A. Negoita, A. Nogga, W. Ormand, P. Sorina, B. Shehadeh, A. Shirokov, J. Spence, I. Stetcu, S. Stoica, T. Weber, and S. Zaytsev, *Eur. Phys. Jour. A* **25**, 475 (2005).
- [53] I. J. Shin, Y. Kim, P. Maris, J. P. Vary, C. Forssén, J. Rotureau, and N. Michel, *Jour. Phys. G: Nucl. Part. Phys.* **44**, 075103 (2017).
- [54] <http://www.nndc.bnl.gov/ensdf>.
- [55] D. Tilley, C. Cheves, J. Godwin, G. Hale, H. Hofmann, J. Kelley, C. Sheu, and H. Weller, *Nucl. Phys. A* **708**, 3 (2002).
- [56] R. J. Charity, J. M. Elson, J. Manfredi, R. Shane, L. G. Sobotka, B. A. Brown, Z. Chajecki, D. Coupland, H. Iwasaki, M. Kilburn, J. Lee, W. G. Lynch, A. Sane-

- tullaev, M. B. Tsang, J. Winkelbauer, M. Youngs, S. T. Marley, D. V. Shetty, A. H. Wuosmaa, T. K. Ghosh, and M. E. Howard, *Phys. Rev. C* **84**, 014320 (2011).
- [57] R. J. Charity, J. M. Elson, J. Manfredi, R. Shane, L. G. Sobotka, Z. Chajecski, D. Coupland, H. Iwasaki, M. Kilburn, J. Lee, W. G. Lynch, A. Sanetullaev, M. B. Tsang, J. Winkelbauer, M. Youngs, S. T. Marley, D. V. Shetty, A. H. Wuosmaa, T. K. Ghosh, and M. E. Howard, *Phys. Rev. C* **82**, 041304 (2010).
- [58] P. Mueller, I. A. Sulai, A. C. C. Villari, J. A. Alcántara-Núñez, R. Alves-Condé, K. Bailey, G. W. F. Drake, M. Dubois, C. Eléon, G. Gaubert, R. J. Holt, R. V. F. Janssens, N. Lécse, Z.-T. Lu, T. P. O'Connor, M.-G. Saint-Laurent, J.-C. Thomas, and L.-B. Wang, *Phys. Rev. Lett.* **99**, 252501 (2007).
- [59] G. Alkhazov, A. Dobrovolsky, P. Egelhof, H. Geissel, H. Irnich, A. Khanzadeev, G. Korolev, A. Lobodenko, G. Münzenberg, M. Mutterer, S. Neumaier, W. Schwab, D. Seliverstov, T. Suzuki, and A. Vorobyov, *Nucl. Phys. A* **712**, 269 (2002).
- [60] I. Tanihata, D. Hirata, T. Kobayashi, S. Shimoura, K. Sugimoto, and H. Toki, *Phys. Lett. B* **289**, 261 (1992).
- [61] I. Tanihata, T. Kobayashi, O. Yamakawa, S. Shimoura, K. Ekuni, K. Sugimoto, N. Takahashi, T. Shimoda, and H. Sato, *Phys. Lett. B* **206**, 592 (1988).
- [62] L. X. Chung, O. A. Kiselev, D. T. Khoa, and P. Egelhof, *Phys. Rev. C* **92**, 034608 (2015).
- [63] P. Müller, L.-B. Wang, K. Bailey, G. Drake, X. Du, J. Greene, A. Heinz, R. Holt, D. Henderson, R. Janssens, C.-L. Jiang, C. Law, Z.-T. Lu, I. Moore, T. O'Connor, R. Pardo, M. Paul, T. Pennington, K. Rehm, and J. Schiffer, *Nuclear Instruments and Methods in Physics Research Section B: Beam Interactions with Materials and Atoms* **204**, 536 (2003), 14th International Conference on Electromagnetic Isotope Separators and Techniques Related to their Applications.
- [64] Z. H. Yang, Y. Kubota, A. Corsi, K. Yoshida, X.-X. Sun, J. G. Li, M. Kimura, N. Michel, K. Ogata, C. X. Yuan, Q. Yuan, G. Authalet, H. Baba, C. Caesar, D. Calvet, A. Delbart, M. Dozono, J. Feng, F. Flavigny, J.-M. Gheller, J. Gibelin, A. Giganon, A. Gillibert, K. Hasegawa, T. Isobe, Y. Kanaya, S. Kawakami, D. Kim, Y. Kiyokawa, M. Kobayashi, N. Kobayashi, T. Kobayashi, Y. Kondo, Z. Korkulu, S. Koyama, V. Lapoux, Y. Maeda, F. M. Marqués, T. Motobayashi, T. Miyazaki, T. Nakamura, N. Nakatsuka, Y. Nishio, A. Obertelli, A. Ohkura, N. A. Orr, S. Ota, H. Otsu, T. Ozaki, V. Panin, S. Paschalis, E. C. Pollacco, S. Reichert, J.-Y. Roussé, A. T. Saito, S. Sakaguchi, M. Sako, C. Santamaria, M. Sasano, H. Sato, M. Shikata, Y. Shimizu, Y. Shindo, L. Stuhl, T. Sumikama, Y. L. Sun, M. Tabata, Y. Togano, J. Tsubota, F. R. Xu, J. Yasuda, K. Yoneda, J. Zenihiro, S.-G. Zhou, W. Zuo, and T. Uesaka, *Phys. Rev. Lett.* **126**, 082501 (2021).
- [65] J. G. Li, N. Michel, H. H. Li, and W. Zuo, *Phys. Lett. B* **832**, 137225 (2022).
- [66] N. Michel, W. Nazarewicz, and M. Płoszajczak, *Nucl. Phys. A* **794**, 29 (2007).
- [67] R. J. Furnstahl and A. Schwenk, *Journal of Physics G: Nuclear and Particle Physics* **37**, 064005 (2010).
- [68] T. Duguet, H. Hergert, J. D. Holt, and V. Somà, *Phys. Rev. C* **92**, 034313 (2015).
- [69] W. Liu, J.-L. Lou, Y.-L. Ye, and D.-Y. Pang, *Nucl. Sci. Tech.* **31**, 2 (2020).
- [70] A. Gade, P. Adrich, D. Bazin, M. D. Bowen, B. A. Brown, C. M. Campbell, J. M. Cook, T. Glasmacher, P. G. Hansen, K. Hosier, S. McDaniel, D. McGlinchery, A. Obertelli, K. Siwek, L. A. Riley, J. A. Tostevin, and D. Weisshaar, *Phys. Rev. C* **77**, 044306 (2008).
- [71] Z. X. Cao, Y. L. Ye, J. Xiao, L. H. Lv, D. X. Jiang, T. Zheng, H. Hua, Z. H. Li, X. Q. Li, Y. C. Ge, J. L. Lou, R. Qiao, Q. T. Li, H. B. You, R. J. Chen, D. Y. Pang, H. Sakurai, H. Otsu, M. Nishimura, S. Sakaguchi, H. Baba, Y. Togano, K. Yoneda, C. Li, S. Wang, H. Wang, K. A. Li, T. Nakamura, Y. Nakayama, Y. Kondo, S. Deguchi, Y. Satou, and K. Tshoo, *Phys. Lett. B* **707**, 46 (2012).
- [72] N. Michel, W. Nazarewicz, M. Płoszajczak, and J. Okołowicz, *Phys. Rev. C* **67**, 054311 (2003).
- [73] J. Lee, X. X. Xu, K. Kaneko, Y. Sun, C. J. Lin, L. J. Sun, P. F. Liang, Z. H. Li, J. Li, H. Y. Wu, D. Q. Fang, J. S. Wang, Y. Y. Yang, C. X. Yuan, Y. H. Lam, Y. T. Wang, K. Wang, J. G. Wang, J. B. Ma, J. J. Liu, P. J. Li, Q. Q. Zhao, L. Yang, N. R. Ma, D. X. Wang, F. P. Zhong, S. H. Zhong, F. Yang, H. M. Jia, P. W. Wen, M. Pan, H. L. Zang, X. Wang, C. G. Wu, D. W. Luo, H. W. Wang, C. Li, C. Z. Shi, M. W. Nie, X. F. Li, H. Li, P. Ma, Q. Hu, G. Z. Shi, S. L. Jin, M. R. Huang, Z. Bai, Y. J. Zhou, W. H. Ma, F. F. Duan, S. Y. Jin, Q. R. Gao, X. H. Zhou, Z. G. Hu, M. Wang, M. L. Liu, R. F. Chen, and X. W. Ma (RIBLL Collaboration), *Phys. Rev. Lett.* **125**, 192503 (2020).
- [74] Y. H. Zhang, H. S. Xu, Y. A. Litvinov, X. L. Tu, X. L. Yan, S. Typel, K. Blaum, M. Wang, X. H. Zhou, Y. Sun, B. A. Brown, Y. J. Yuan, J. W. Xia, J. C. Yang, G. Audi, X. C. Chen, G. B. Jia, Z. G. Hu, X. W. Ma, R. S. Mao, B. Mei, P. Shuai, Z. Y. Sun, S. T. Wang, G. Q. Xiao, X. Xu, T. Yamaguchi, Y. Yamaguchi, Y. D. Zang, H. W. Zhao, T. C. Zhao, W. Zhang, and W. L. Zhan, *Phys. Rev. Lett.* **109**, 102501 (2012).
- [75] I. Brida, S. C. Pieper, and R. B. Wiringa, *Phys. Rev. C* **84**, 024319 (2011).
- [76] F. Beck, D. Frekers, P. von Neumann-Cosel, A. Richter, N. Ryezayeva, and I. Thompson, *Phys. Lett. B* **671**, 496 (2009).
- [77] A. H. Wuosmaa, J. P. Schiffer, K. E. Rehm, J. P. Greene, D. J. Henderson, R. V. F. Janssens, C. L. Jiang, L. Jisonna, J. C. Lighthall, S. T. Marley, E. F. Moore, R. C. Pardo, N. Patel, M. Paul, D. Peterson, S. C. Pieper, G. Savard, R. E. Segel, R. H. Siemssen, X. D. Tang, and R. B. Wiringa, *Phys. Rev. C* **78**, 041302 (2008).